

RITMOS: a micromirror-based multi-object spectrometer

Reed D. Meyer^a, Kevin J. Kearney^b, Zoran Ninkov^a, Christopher T. Cotton^c,
Peter Hammond^d, and Bryan D. Statt^c

^aRochester Institute of Technology, Center for Imaging Science, 54 Lomb Memorial Drive,
Rochester, NY, USA 14623;

^bPixel Physics, Inc., 125 Tech Park Drive, Rochester, NY, USA 14623;

^cASE Optics, Inc., 2 Stony Ridge Drive, Honeoye Falls, NY, USA 14472;

^dLightforce Technology, Inc., 125 Tech Park Drive, Rochester, NY, USA 14623

ABSTRACT

The Rochester Institute of Technology Multi-Object Spectrometer (RITMOS) utilizes a Texas Instruments Digital Micromirror Device (DMD) for target selection, instead of the fiber bundles or customized slit masks normally used in multi-object spectroscopy. The DMD, which sits at the telescope focal plane, is an 848×600 array of 17 micron square mirrors that can individually deflect incident light into one of two output paths: an imaging path or a spectroscopy path. In standard operation, all light is deflected towards the imaging path, consisting of an Offner relay which reimages the DMD onto a CCD detector. The locations of spectroscopic targets are then noted, and the micromirrors corresponding to these targets are then deflected towards the spectroscopy path. This path utilizes a 1200 1/mm transmission grating to disperse images of the micromirror pattern onto a second CCD detector. The spectroscopic parameters (e.g., 0.66 Å/pixel dispersion for a 13.5 micron/pixel detector) were chosen for MK spectral classification. Among the benefits of replacing a fiber bundle or custom slit mask with a DMD are the latter's instantaneous reconfigurability and its aptitude for the study of compact fields. RITMOS is thus suited towards spectral classification surveys of star clusters. We present a description of the instrument, details of its design, and initial measurements, including multi-object stellar spectra.

Keywords: astronomical instrumentation, spectroscopy, Digital Micromirror Devices, microelectromechanical systems, spectral classification

1. INTRODUCTION

Recent innovations in microelectromechanical systems (MEMS) technology are now being applied to the realm of astronomical data acquisition. One MEMS innovation is an array of miniature mirrors, developed by Texas Instruments and called a Digital Micromirror Device (DMD).¹ A common DMD format, "SVGA," is an array of 848×600 mirrors, each of which is $16 \mu\text{m}$ on a side, with $17 \mu\text{m}$ between centers. The micromirrors can individually tilt 10° in either direction relative to the normal to the array.² The mirrors are independently programmable via a computer interface, and they can be switched between their two positions as rapidly as thousands of times per second. The DMD is a key component in commercial projection systems utilizing Digital Light Processing (DLP) technology, and it is in that and similar applications where they have enjoyed most of their use.

But micromirror arrays also have a natural application to multi-object spectroscopy, and specifically to the problem of selecting targets from a two-dimensional sky field for simultaneous spectral acquisition. With the sky field imaged on a DMD, a small subset of the DMD's mirrors, located at the positions of interesting targets

Further author information: (Send correspondence to R.D.M.)

R.D.M.: rdmpci@cis.rit.edu; telephone 1 585 475-2217; FAX 1 585 475-5988

K.J.K.: kevin.kearney@pixelphysics.com; telephone 1 585 427-8310; FAX 1 585 427-8422

Z.N.: ninkov@cis.rit.edu; telephone 1 585 475-7195; FAX 1 585 475-5988

C.T.C.: chrisc@aseoptics.com; telephone 1 585 303-1574; FAX 1 585 624-8083

P.H.: phammond@lightforcetech.com; telephone 1 585 292-5610; FAX 1 585 427-8422

B.D.S.: bryans@aseoptics.com; telephone 1 585 303-1574; FAX 1 585 624-8083

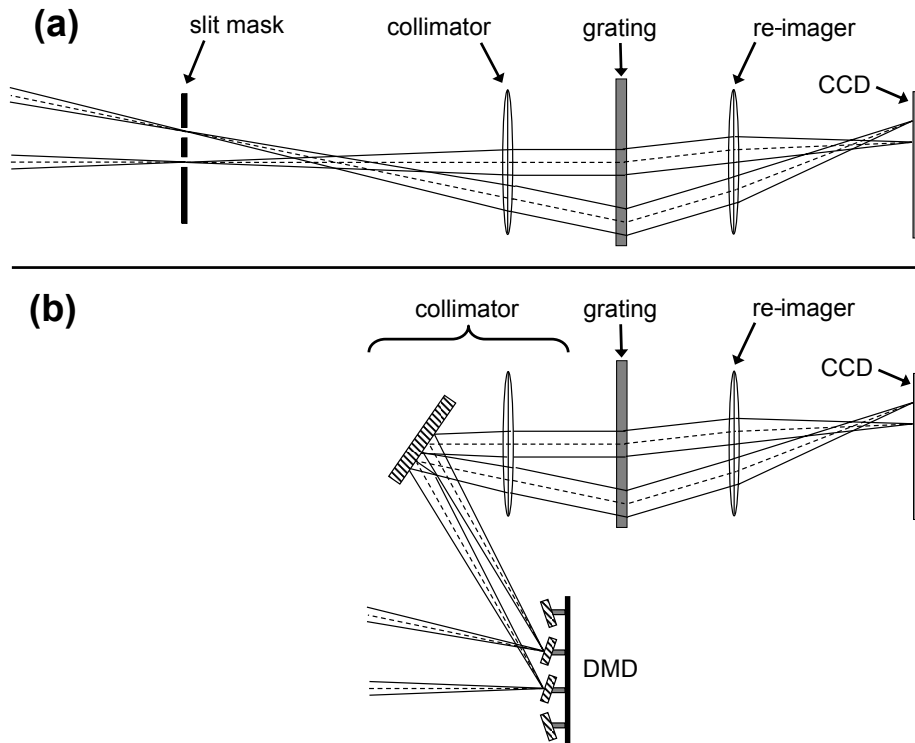


Figure 1. A comparison between a MOS that uses a slit mask for target selection and a DMD-based MOS. **(a)** The essential layout of a MOS that has a conventional slit mask at the telescope focal plane. Two slits are shown, and their beams pass through a collimator, a grating, and a re-imager before the dispersed light is focused on a detector such as a CCD. The placement of optical elements and light rays, and the use of transmissive optics, was chosen for illustrative purposes only; for example, the beams would be much wider in a typical spectrograph, and the grating would usually be reflective. **(b)** The same as **(a)**, but for a DMD-based MOS such as RITMOS. Here a micromirror array has replaced the slit mask, and two mirrors are shown deflecting their light towards the collimator, while the other mirrors are tilted at the opposite angle.

in the field, can be commanded to deflect light towards a spectrograph, while the remaining mirrors deflect the rest of the field in a different direction. In this way, the DMD may take the place of the optical fiber bundles or customized slit masks conventionally³ used for target selection in multi-object spectroscopy. IRMOS,⁴ a multi-object spectrograph (MOS) currently under development, will utilize a DMD for near-infrared observations. We have produced a DMD-based MOS that works at optical wavelengths, particularly the 3900–4900 Å regime that is the domain of MK spectral classification. In this paper we describe this instrument, “RITMOS,” and we present its optomechanical and electronic design, and initial measurements that confirm the design, including multi-object astronomical observations. Early concepts for a MOS utilizing DMD technology, and an initial characterization of DMD optical properties, were presented in Ref. 5.

Figure 1 illustrates the conceptual differences between RITMOS and a MOS that uses a conventional slit mask, such as GMOS.^{6,7} Figure 1a shows the basic layout of the latter type of MOS, including the slit mask, located at the telescope’s focal plane; a collimator; a grating; re-imaging optics; and a two-dimensional detector, on which the spectrally dispersed slit mask is imaged. For simplicity here, the grating is considered a transmission grating, although it is usually a reflective grating in practice. Figure 1b shows the basic layout of the DMD-based RITMOS. Note that the primary difference between the two arrangements is the method of slit construction at the focal plane: in RITMOS, a DMD replaces the slit mask of Figure 1a or the entrance apertures of fiber bundles in a fiber-based MOS. On the micromirror array, filled rectangular regions of mirrors are tilted to deflect incident light towards a spectrograph, while the surrounding mirrors deflect light in a different direction. These

rectangular regions, when positioned at the locations of spectroscopic targets on the focal plane, function like the slits occupying a slit mask, and henceforth will be called “slits” in this document. Because the DMD’s slits are reflective rather than clear apertures, the configuration of the next element in the system, the collimator, differs somewhat between the DMD and slit mask MOS layouts, as noted in Figure 1.

In RITMOS, the micromirrors that do not tilt towards the spectrograph deflect light towards an imaging channel, which reimages the DMD onto a CCD detector. In this way the telescope’s focal plane, minus those areas where micromirrors are tilted towards the spectrograph, may be imaged concurrently with any spectroscopic exposures. The duplexing nature of the DMD confers increased telescope efficiency when a field requires, for example, both photometry and spectroscopy: slits are placed on certain targets for spectroscopic observation while the remaining field is imaged, and subsequent slit patterns are arranged to spectrally acquire the remainder of the field. But the primary purpose of the imaging channel is to locate spectroscopic targets in order to precisely place DMD slits. Under normal operation, all DMD mirrors are initially tilted towards the imaging channel, in order to image the entire field; the locations of targets of spectroscopic interest are noted in the ensuing image; and then slits are formed on the DMD at the locations of those targets in the focal plane. This procedure obviates the need to perform precise astrometry of the targets in advance of observations, a significant concern with conventional MOS techniques.

The imaging channel, in conjunction with the rapid reconfigurability of the DMD, also eliminates the need to arrange the slits well in advance of observations. For example, with GMOS, the field must be imaged with the same instrumentation about one month before the spectroscopic observations, to allow time to construct the mask.⁸ For both slit mask and fiber-based spectrographs, valuable telescope time is often spent swapping masks or reconfiguring fibers between observations; for example, Hydra⁹ often requires 25 minutes or more to completely reposition its fibers.¹⁰ In RITMOS, it takes about 0.5 s to transfer a complete micromirror pattern to the DMD, rendering slit reconfigurations effectively instantaneous. If the observer errs in configuring the slits or has a sudden need to change the pattern, due to a target of opportunity for example, it is trivial to upload a new pattern to the DMD.

The DMD can display any conceivable pixel pattern—slits are not limited to a specific width or height, nor must they even be rectangular in shape. This is advantageous with respect to fiber-based spectrographs, since the entrance apertures of fibers are fixed in both size and shape, and the fibers’ cladding imposes a minimum separation between targets that can be substantial unless a compact fiber bundle is specifically employed. Fiber placement on the focal plane is also generally limited—fibers often may not cross or may move in certain directions only. The throughput losses in a DMD, due to its window and to a single reflection off of an aluminum micromirror, are considerably less than the losses in the fibers and their couplings in a fiber-based MOS.

The substitution of a DMD for robotic fibers or for a slit mask exchanger also offers a lighter, more compact, less expensive spectrograph that is more robust because it requires fewer moving parts. These were leading motivations in the choice of a DMD for IRMOS, as it was a ground-based testbed for a MOS for the James Webb Space Telescope.⁴ RITMOS is small and light enough to mount directly to the Mees Observatory 24” Cassegrain telescope owned and operated by the University of Rochester. The DMD itself is mechanically reliable, with a projected lifetime in excess of 100,000 hours under normal operating temperatures.^{2, 11}

Because the micromirrors can rapidly toggle between states, a DMD can also increase the effective well depth of a CCD used for spectroscopic exposures. Slits on bright sources can be toggled “off” intermittently, while faint sources accumulate counts throughout a long exposure; assuming a sufficient time in the “off” state, the bright sources will not saturate the detector.

The use of a micromirror array is not without disadvantages. Of perhaps the greatest concern is scattered light due to at least two phenomena. It has been shown that the array of micromirrors, much like a reflection grating, has a strong diffraction pattern.⁵ Another source of scattering is incident light that lands in the gaps between micromirrors and reflects off the metal substrate. The baffles in RITMOS block much but not all of the scattered light; the remainder results in a measureable switching contrast between the “on” and “off” states of a micromirror. Switching contrast is also a concern with IRMOS.⁴ The size of the DMD, 14.4 mm×10.2 mm, also limits the field of view available to RITMOS, although Texas Instruments has introduced progressively larger DMD formats since the release of the 848 × 600 chip.²

The properties of a micromirror array functioning as a slit mask suggest that the DMD is well suited towards spectroscopy of star clusters. We decided that a first-generation DMD-based MOS should address spectroscopic programs that do not require high spectral dispersion and resolution. MK spectral classification is such a program, and its application towards open clusters remains a largely untapped source of a variety of astrophysical data. It is a means of deducing spectral types directly, without the reddening concerns that affect photometric methods. Therefore, the spectral resolution and wavelength coverage of RITMOS were optimized for high-precision surveys of the MK spectral types of star clusters. The instrument's spectroscopic parameters are also appropriate for studies of stellar activity of cluster members. RITMOS is generally applicable to investigations requiring multi-object or imaging spectroscopy at moderate spectral dispersion and at blue wavelengths.

2. SPECIFICATIONS

We estimated that the determination of MK spectral types with high precision requires a spectral resolution of $\sim 1 \text{ \AA}$ at 4400 \AA , and a dispersion of $\sim 0.66 \text{ \AA/pixel}$ on the spectroscopic CCD. The former specification was to ensure resolution of certain metal lines, and the latter was to guarantee that the minimum wavelength range of $3900\text{--}4900 \text{ \AA}$ would be captured by a detector no narrower than 2048 pixels, while simultaneously sampling the delivered spectrum at nearly the Nyquist frequency. The $3900\text{--}4900 \text{ \AA}$ range is the classic domain of MK spectral classification; the effective number of CCD pixels available to cover this minimum range is less than 2048, because spectra delivered from opposite corners of the DMD are shifted substantially with respect to each other in the dispersion direction. The fact that the two competing interests of wavelength range and sampling rate could nevertheless both be met is a fortunate result of the resolution specification being $\sim 1 \text{ \AA}$. The CCD pixel size expected for most of the spectroscopic work is $13.5 \mu\text{m}$ square, which fixes the desired dispersion to 48.6 \AA/mm .

Conditions specific to Mees Observatory, which was to serve as the testbed and initial source of astronomical data for RITMOS, defined the remaining parameters. The Mees $24''$ Boller and Chivens telescope delivers an $f/13.5$ beam at the Cassegrain focus, but the corresponding plate scale ($25''/1/\text{mm}$), coupled with the sizeable seeing that had been expected at Mees ($\sim 2''\text{--}2''5$), would require a slit approximately five micromirrors wide to match the typical PSF. Since the collimator in the core commercial subsystem (see §3.1.1) accepts beams as fast as $f/6.9$ without light loss from the conservation of etendue, we added foreoptics to demagnify the telescope beam to a value slightly slower than $f/6.9$, so as to not only require fewer micromirrors per stellar image, but also to cover a broader field of view. The f -number in the final design is $f/7.62$. This sets the plate scale at Mees to $44''/4/\text{mm} = 0''755$ per DMD pixel, and the field of view to $10'7 \times 7'6$. With this plate scale, two micromirrors ($33 \mu\text{m}$) subtend $1''47$, which roughly matches the core of the expected PSF, so a two-mirror-wide slit was selected as the nominal slit width for the spectrograph design. Slit widths equal to any integer number of micromirrors are possible, but the spectral resolution requirement was specified for two mirrors. RITMOS observations have typically experienced seeing of $\sim 3''\text{--}3''5$, so somewhat larger slits have been used in practice. Fortunately, larger slit width is compensated by an increased resolution in the final design; the resolution had been changed from 1 \AA to 0.703 \AA , under the estimation that placing approximately 0.93 resolution elements per pixel would sample the spectrum adequately.

RITMOS is intended for other telescopes besides Mees. Larger telescopes will generally have smaller plate scales, necessitating wider slits, but this is mitigated somewhat by better seeing conditions at most such sites. An example telescope is the WIYN Observatory, whose Nasmyth focal plane has a plate scale of $9''374/\text{mm}$, and which delivers a median seeing of $\sim 0''7$.¹² For WIYN, a slit three micromirrors ($50 \mu\text{m}$) in width may be appropriate, as it would subtend $0''469$, or about 67% of the seeing FWHM, with 1:1 foreoptics. Such a slit has a predicted resolution of 1.07 \AA , which should be quite adequate for MK spectral classification.

As implied by §1, the slit width can be quickly changed to match fluctuations in seeing—even during an exposure, if required. The predicted spectral resolution $\Delta\lambda$ is approximately $0.0213 \cdot s \text{ \AA}$, for a general slit width s in microns. Since the micromirrors are $16 \mu\text{m}$ wide on $17 \mu\text{m}$ centers, $\Delta\lambda \simeq 0.0213(17n - 1) \text{ \AA}$, where n is a positive integer. That is, $\Delta\lambda$ may be chosen from 0.341 \AA , 0.703 \AA , 1.07 \AA , 1.43 \AA , \dots , with the choice influenced by the size of the target on the DMD.

Table 1 summarizes the primary specifications used in the final optical design, including the requirement that the optical quality be limited by the atmosphere, not by the internal optics. There were many other

Table 1. Primary optical specifications for RITMOS.

Spectroscopy	
Purpose	multi-object high precision MK spectral classification
Central wavelength	4400 Å
Delivered wavelength range	3900–4900 Å, minimum*
Resolution	0.703 Å @ 4400 Å for a two-mirror-wide DMD slit ($\lambda/\Delta\lambda = 6260$)
Dispersion	48.6 Å/mm (0.656 Å/pixel for a detector with 13.5 μm pixels)
Design parameters specific to Mees Observatory	
Optical quality	atmosphere limited
Foreoptics	feed the DMD with an f/7.62 beam
Plate scale	44''/mm = 0''755/pixel at the DMD
Field of view	10'7 × 7'6 (entire DMD is illuminated)

*Minimum range delivered to a 2048 × 13.5 μm wide detector from any mirror on the DMD

requirements imposed upon the optics, mechanics, and other aspects of the instrument. Throughput loss due to optical mismatch was to be minimized, as implied above. Wavelength calibration was to be provided through an onboard krypton lamp subsystem. Efforts were to be employed to minimize scattering by a system of baffles, flexure by using thick aluminum plates in a sturdy arrangement, and light leakage by overlapping plates and sealing gaps. Electronic control was to be delegated to a PC in an observatory warm room, on which would run a user interface that would provide easy creation of slit patterns optimized for multi-object spectral acquisition. The next section describes how we met these requirements and others.

3. DESIGN

3.1. Optics

3.1.1. Optical design overview

Figure 2 shows the “optical bench” that constitutes the main enclosure in RITMOS. It shows the optical paths of the imaging channel and the spectroscopy channel within the overall layout of the instrument. Figures 3 and 4 focus on the spectroscopy channel and the imaging channel, respectively, showing the behavior of the optical beams in greater detail. Figure 5 offers a different view of the interior, and demonstrates the 45° rotation of the DMD, which is covered in §3.1.3.

Referring to Figure 2, the telescope focal plane is re-imaged onto the DMD by the foreoptics assembly. The foreoptics can be interchanged to adapt to different telescopes and different desired magnifications of the plate scale. Initially, all mirrors are tilted so as to direct light into the imaging channel (the right side of Figure 2). The light reflects from the DMD to a fold mirror, and is then redirected to a two-mirror 1:1 Offner image relay. A second fold mirror redirects light from the Offner relay through a filter wheel and onto the imaging CCD. As discussed below, the CCD is oriented so as to correctly focus the tilted image plane.

Once the scene is recorded by the imaging CCD, target objects are identified and the micromirrors corresponding to those object positions on the DMD are tilted so as to direct light to the spectroscopy channel (the left side of Figure 2). All remaining micromirrors are left unchanged. A three-mirror, all-reflective collimator directs the light through a planar transmission grating, whence the light passes through the re-imaging lens system and onto the spectroscopic CCD.

A spectroscopic integration is taken and read out of the CCD. The DMD mirror configuration is left unchanged, and the calibration lamp assembly is actuated so as to block light from the telescope and illuminate the DMD with fiber-coupled light from a krypton discharge lamp located in the electronics enclosure. A second spectral integration is recorded. This process provides reference spectra immediately following acquisition of stellar spectra.

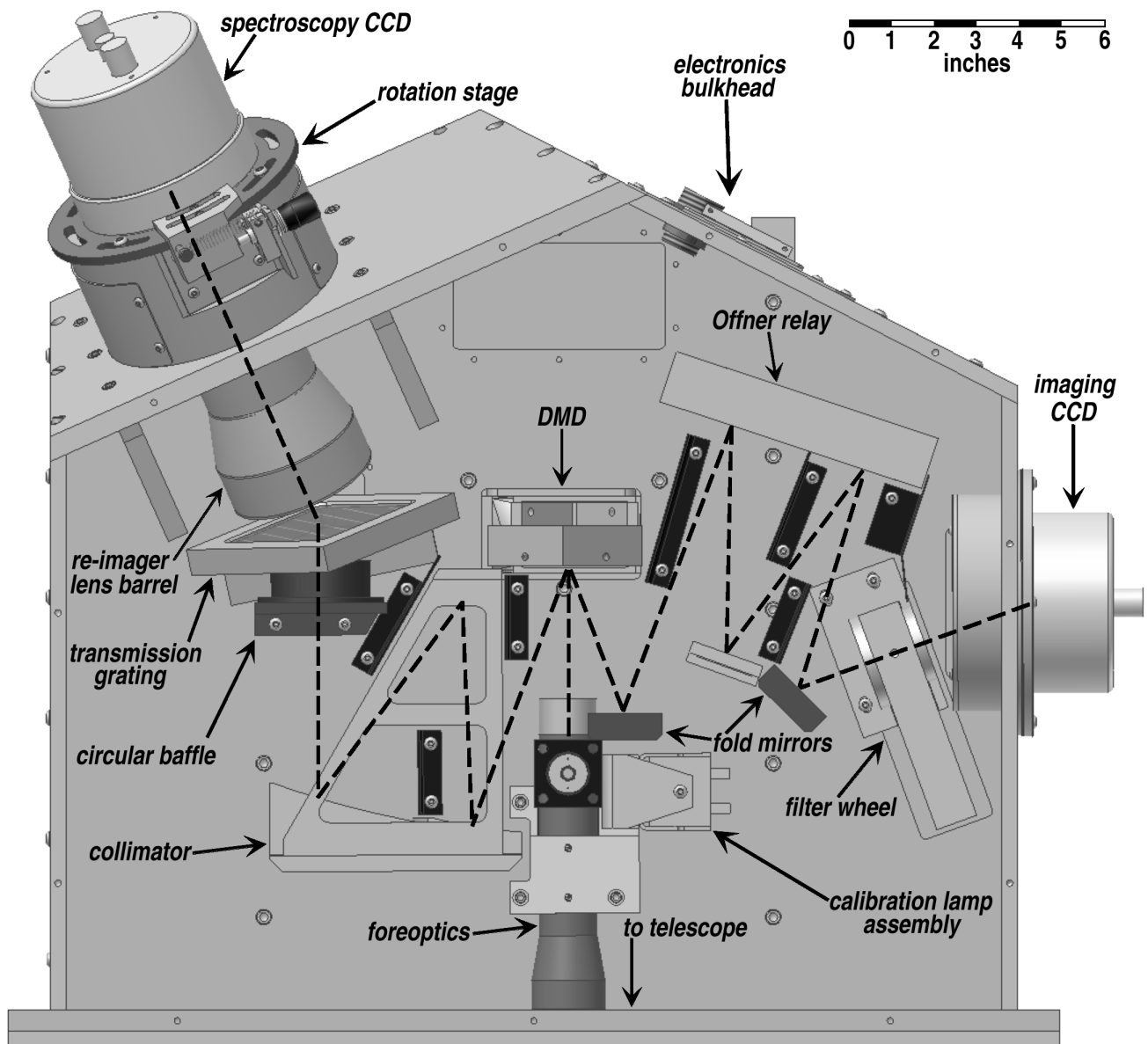


Figure 2. Top view of the optical bench of RITMOS. This CAD drawing of the main interior contains all mechanical elements visible from this direction except for a horizontal reinforcement brace and electrical and fiber-optic cables. The black rectangles are mounts for thin baffles which stand perpendicular to the page. The dashed lines indicate the optical paths. Light enters the instrument from the bottom wall, which faces the telescope; the light passes through the foreoptics and encounters the DMD near the center of the Figure. Here the optical path bifurcates, with the left branch heading towards the spectroscopy channel and the right branch towards the imaging channel. The spectroscopy channel includes a collimator with three reflections, a grating, a re-imager, and the spectroscopy CCD. The imaging channel includes two fold mirrors, an Offner relay, a filter wheel, and the imaging CCD. The calibration lamp assembly adjoins the foreoptics.

The core optical design of RITMOS is based on a subsystem now available commercially from Pixel Physics, Inc., located in Rochester, NY. This core includes the DMD, as well as the all-reflective Offner relay and collimator subsystems, and is designed to be achromatic across the entire visible spectrum. As discussed below, the core design also accommodates the requirement to operate with the tilted image plane of the DMD. Since RITMOS was designed for MK spectral classification, it did not require the broad optical bandwidth of the core design.

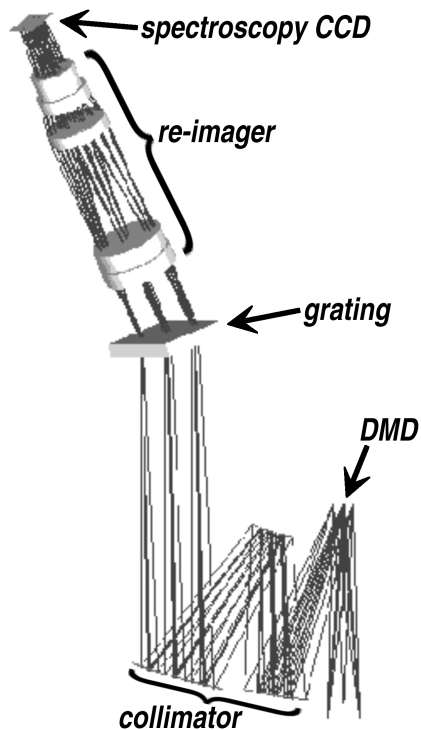


Figure 3. Optical model of the spectroscopy channel. Light passes from the DMD to a three-mirror collimator, and thence to a transmission grating. A five-element lens system re-images the dispersed light on the spectroscopy CCD. Optical beams from three field angles are visible.

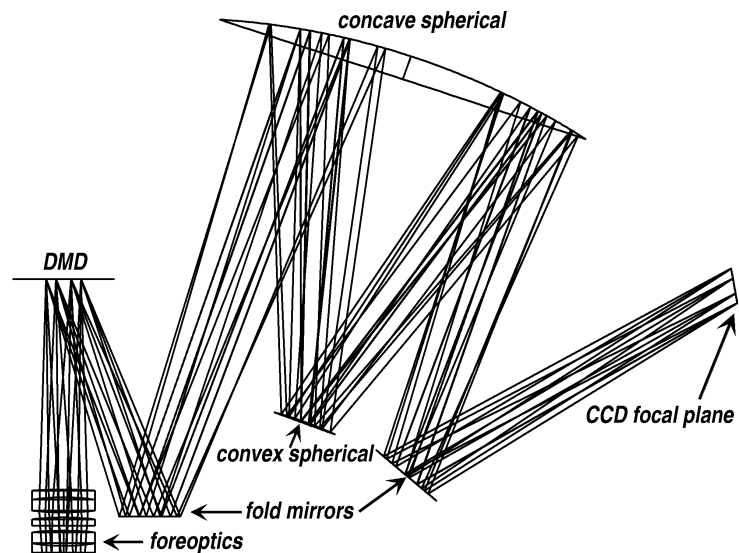


Figure 4. Optical model of the imaging channel. An Offner relay, consisting of spherical mirrors, re-images the DMD onto the imaging CCD with nearly 1:1 magnification. Two flat mirrors fold the beam. The 20° angle between the DMD plane and the emergent beam requires the final beam to intersect the CCD focal plane at the same oblique angle.

Hence, a transmission grating was used for dispersion, and a refractive system was designed for the re-imager. The resulting optical system has demonstrated excellent image quality and spectral resolution.

3.1.2. Imaging channel

The all-reflective relay that is used to re-image the DMD to the imaging CCD consists of two concentric spherical mirrors with a common center of curvature. It is well known that an object that is at the center of curvature of a spherical mirror is perfectly imaged without optical aberrations. In the Offner design,¹³ the larger mirror has a concave radius of curvature that is twice that of the convex smaller mirror (see Figure 4). The object is located at the common center of curvature, but laterally offset. The lateral offset does not have a significant negative effect on the image quality of the system, as the optical aberrations continue to be close to zero as the image moves off-axis. The only residual aberration is astigmatism, which is easily corrected by slightly adjusting the spacing between the two mirrors.

This type of afocal relay is ideal for relatively compact 1:1 imaging systems, and introduces no chromatic aberrations. In addition, a 1:1 magnification afocal relay has the property of maintaining unit magnification for objects in and out of the conjugate planes. Since the DMD micromirrors tilt at $\pm 10^\circ$, light incident from the telescope along the DMD normal is reflected at $\pm 20^\circ$ from the normal. Hence the image relay views the DMD as tilted with respect to the object plane, and re-images it as a tilted image plane. The 1:1 Offner design re-images this tilted object plane onto the imaging CCD with no magnification distortion. Note, however, that the imaging CCD is required to be tilted at 20° to match the tilt of the focused image plane.

The particular Offner relay incorporated into RITMOS is designed to operate at f/8.5 and has been optically modelled using the ZEMAX package available from ZEMAX Development Corporation in San Diego, CA. The



Figure 5. The interior of RITMOS, as viewed from the top front corner on the imaging side. The diamond-shaped structure at the center houses the DMD, which is the lighter area within the structure. The DMD is rotated so that the mirror diagonals are perpendicular to the primary optical plane. In the left foreground is the calibration lamp assembly; behind that, from front to back, are the collimator, the grating, and the re-imager lens barrel. The grating, like the DMD, is rotated by 45° . Both the grating and the lens barrel are tilted up from the primary optical plane. The spectroscopy CCD is visible above the back wall, behind the lens barrel. The Offner relay is to the right of the DMD.

models show that the relay maintains a spot size that is less than $8 \mu\text{m}$ in diameter over the entire field of view of the DMD. They also indicate that the distortion is well controlled, never exceeding 0.1%. A ray trace calculation of the performance of the imaging channel is shown in Figure 6. The figure shows spot diagrams for three field angles, with each spot superposed with a projected DMD pixel. As is evident, the spatial resolution of the imaging channel is limited by the $17 \mu\text{m}$ DMD pixels. The diagram also shows a circle of diameter $14.54 \mu\text{m}$, which represents the smallest PSF, in linear units, that any telescope is ever likely to deliver to RITMOS—it corresponds to $0''.5$ seeing at a telescope with a focal length of 6 m. A longer focal length telescope delivers a spatially larger PSF, whereas RITMOS would probably not be used with a shorter telescope. The relative size between this circle and the spot indicates that the spatial resolution of the imaging channel will always be atmosphere-limited.

Control of stray light in an Offner relay is very important because of the direct image path from the object to the large mirror. The baffles in the system have been arranged to reduce stray light effectively.

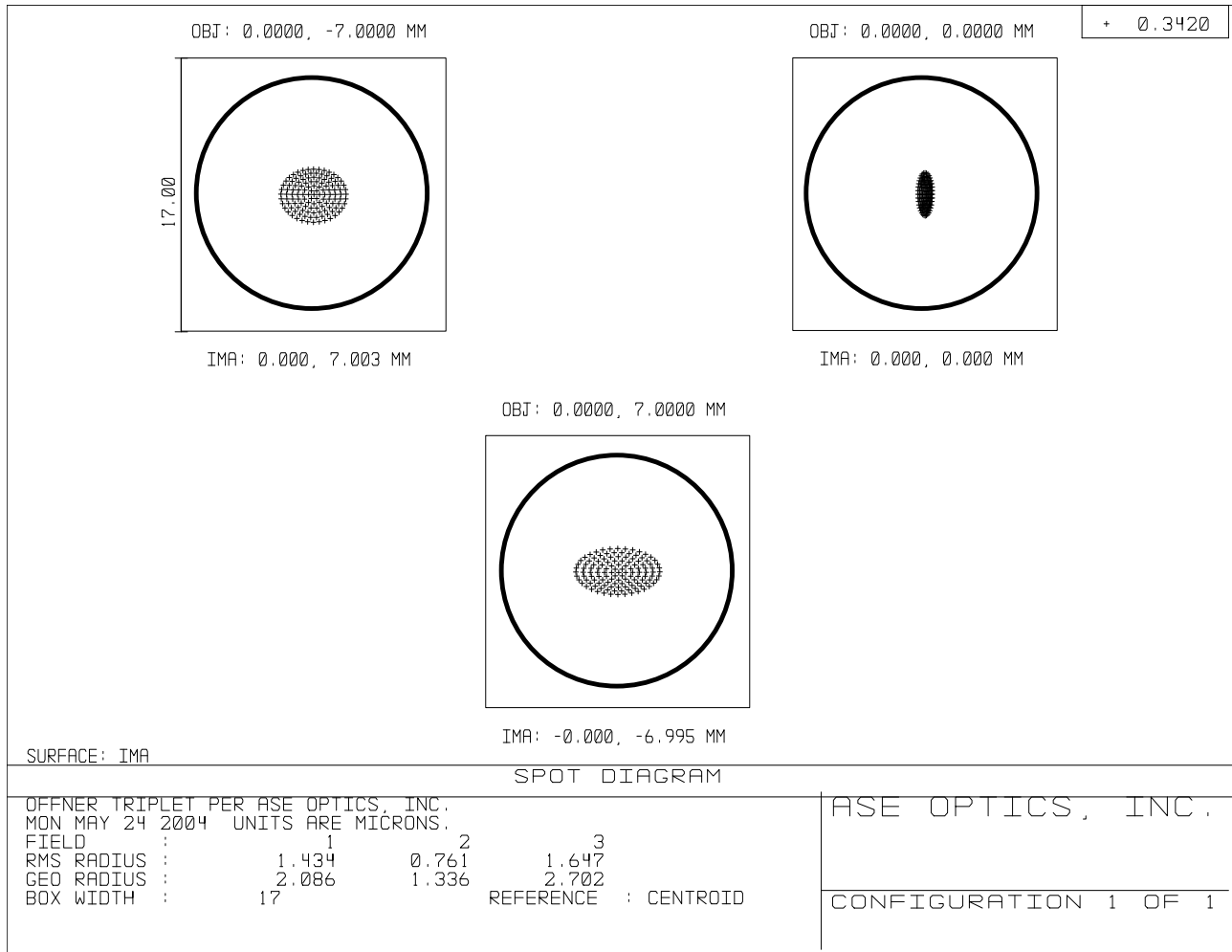


Figure 6. ZEMAX point spread model for the imaging channel, consisting of ray traces from three points on the DMD: the center and two points $\sim 80\%$ of the distance to the DMD corners. The $17\ \mu\text{m}$ square on each spot represents one DMD pixel, virtually unmagnified by the Offner relay. The thick circle centered on each spot has a diameter of $14.54\ \mu\text{m}$, which corresponds to a $0''.5$ seeing disk for a telescope with a focal length of 6 m and no intervening magnification. Because the Offner relay is nearly achromatic, the spot diagrams, here for $3420\ \text{\AA}$, are similar for other wavelengths of interest.

3.1.3. Spectroscopy channel

The spectroscopy subsystem consists of an off-axis reflective collimator, a diffraction grating that operates in transmission, and a re-imaging lens. The system magnification from the DMD to the spectroscopy CCD is approximately 0.44, because the collimator operates at $f/7.62$ and the re-imager operates at $f/3.35$.

The off-axis reflective collimator is a three-mirror aspheric system, consisting of diamond-turned, nickel-plated aluminum. It produces a collimated output beam with an offset exit pupil that is located at the diffraction grating. As with the imaging channel, this collimator design accommodates the fact that the DMD is tilted at 20° with respect to the optical axis. Over the field of view of the DMD, the reflective system is diffraction limited and is predicted to have a geometric distortion of less than 0.2%. Maintaining diffraction-limited wavefront performance at the grating is important to limit the aberrations that are introduced by a mismatch of angles at the diffraction grating.

A transmission grating was chosen for the system in order to reduce the space requirements while maintaining reasonable diffraction efficiency. The 1200 l/mm grating, from Spectra-Physics RGL in Rochester, NY, is 70 mm

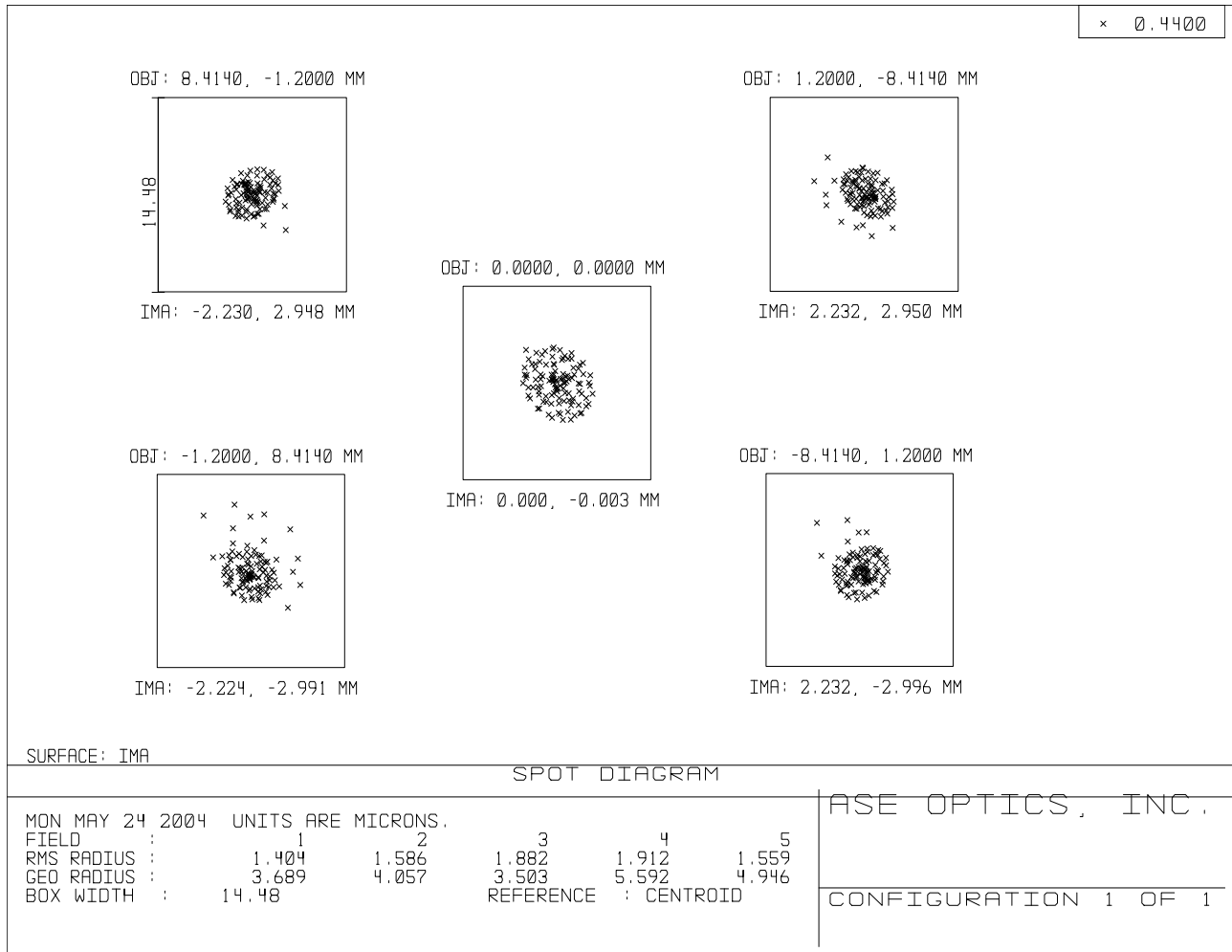


Figure 7. ZEMAX point spread model for the spectroscopy channel, consisting of ray traces from the DMD center and its four corners to the spectroscopy focal plane. The square centered on each spot represents the approximate projection of a 2×2 micromirror subarray, i.e., the nominal slit width. The simulation wavelength is 4400 \AA .

square, has a BK7 substrate, and is blazed for $\sim 4000 \text{ \AA}$ wavelength. Because the grating operates in the first order and the reddest wavelength in the design specification is 4900 \AA , the spectroscopy channel requires no order-sorting filter.

The DMD has square micromirrors that tilt about their individual diagonals. For this reason the DMD needs to be rotated at 45° with respect to the plane of symmetry of the Offner relay and the reflective collimator. Figure 5 shows this rotation. Removal of this rotation from the imaging and spectroscopy focal planes is accomplished by simply rotating the two detectors to match the rotation of the DMD. It is additionally desirable to rotate the dispersion angle such that the dispersion is perpendicular to the long axis of the DMD. This maximizes the number of targets for simultaneous spectral acquisition, and is achieved by rotating the grating by 45° , such that the grooves of the grating are parallel to the long dimension of the DMD.

As discussed above, the re-imager is a refractive system, designed to provide the low f -number that is required to achieve the 0.44x magnification from the DMD to the imaging CCD, while maintaining an effective field of view of 2° to cover the spectral dispersion. The refractive system has five elements in three groups and is designed to be chromatically corrected over the wavelengths of interest ($3900\text{--}4900 \text{ \AA}$). The re-imager is not designed to be diffraction limited, but rather is designed to match the smallest expected CCD pixel size of 9 \mu m . Figure 7 shows

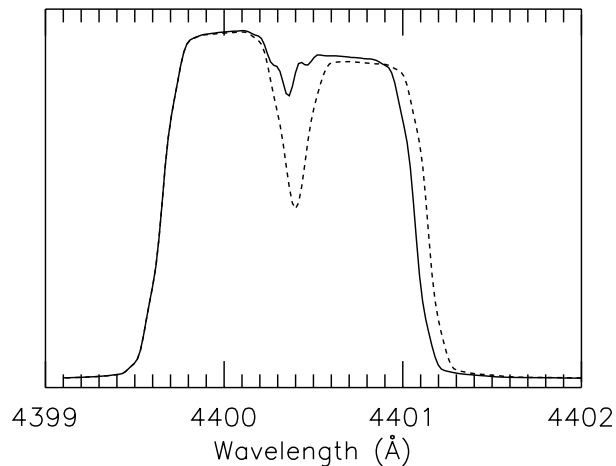


Figure 8. Spectral resolution prediction from the ZEMAX model of RITMOS. A source consisting of delta functions at 4400 Å and $(4400 + \Delta\lambda)$ Å uniformly illuminated a two-mirror-wide slit at the DMD center. The solid curve is for $\Delta\lambda = 0.7033$ and the dashed curve is for $\Delta\lambda = 0.7736$. The heights of the two spectral lines were arbitrary in the simulation.

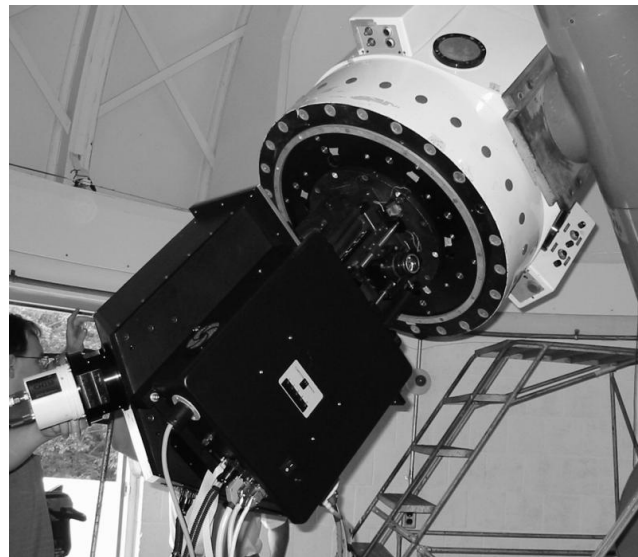


Figure 9. RITMOS mounted to the Mees Observatory 24" telescope. The electronics module is in the foreground; behind it is the optics enclosure, with the spectroscopic CCD pointing to the left. The instrument is attached directly to the Mees offset guider, which in turn is mounted to the bottom of the primary mirror cell of the telescope. Photograph taken 2003 August 8 during the initial installation at Mees.

a ray trace calculation of the spot diagram at the 4400 Å center wavelength for several field angles. Superposed on each spot diagram is a $\sim 14.5 \mu\text{m}$ box, which represents a projected 2×2 DMD slit; a two-micromirror-wide, or $33 \mu\text{m}$, slit is the nominal slit width listed in the table of design specifications (Table 1). The spots are significantly smaller than the projected slit width, i.e., the spectral resolution is dominated by the slit, not by the spectroscopy channel's internal optics.

For the slit-dominated case, the standard expression for a spectrometer's resolution, $\Delta\lambda$, is the dispersion times the projected slit width.¹⁴ This yields $\Delta\lambda = 0.7033 \text{ Å}$ for a two-mirror-wide slit with RITMOS. Figure 8 shows predictions of the spectral resolution at the spectroscopy focal plane, prior to degradation due to detector sampling. In the curve for $\Delta\lambda = 0.7033 \text{ Å}$, the two spectral lines are just barely resolved, in agreement with the standard expression for $\Delta\lambda$. In the other simulation, denoted by the dashed curve in the figure, $\Delta\lambda$ was increased by 10%, to 0.7736 Å . Here the lines are clearly resolved.

3.1.4. Calibration assembly

The calibration assembly provides an *in situ* reference spectrum. A solenoid-driven slide mechanism inserts the assembly into the foreoptics lens barrel. When retracted, the lens barrel aperture is open, allowing light from the telescope to enter the system. When inserted, the calibration assembly blocks light from the telescope. A krypton calibration lamp (Oriel Instruments Spectral Calibration Lamp, model 6031), located in the electronics enclosure, is optically coupled to one end of a multimode fiber optic cable. The other end of the fiber-optic cable injects light into the assembly; this light is nominally collimated by a plano-convex (PCX) lens and then redirected by a first-surface right-angle mirror through a light shaping diffuser (LSD) from Physical Optics Corp., Torrance, CA. An LSD is a randomized surface relief structure that enables controlled angular distribution of incident light. The calibration assembly is inserted such that the LSD is positioned inside the lens barrel near the exit pupil position. By choosing the correct LSD angular specifications and the fiber-PCX separation, the result is to uniformly illuminate the DMD with a field angle and divergence matching those of the light from the telescope-foreoptics pair.

As discussed in §3.1.1, the calibration assembly is typically used to capture a reference spectrum immediately following acquisition of target spectra. Since the DMD mirrors are left in the exact configuration used during the target spectral acquisition, the calibration can be performed immediately. The calibration assembly may also be used to illuminate the entire DMD to check micromirror configurations via the imaging CCD. In this manner the operator can perform a DMD status check remotely from the control room.

3.2. Mechanics

The mechanical design emphasis was placed on minimizing flexure, albeit at the expense of weight. The main supporting structure is a flat and sturdy baseplate. The baseplate also defines the primary optical plane within RITMOS. The baseplate is supported by two rails fastened to its underside; in addition to stiffening the baseplate, these rails also provide mounting surfaces to attach the separate electronics cabinet. The sidewalls add strength to the enclosure and are overlapped at each mating edge to eliminate light leakage. The top cover also overlaps all mating wall edges and is easily removed for access to the optical components. The optical components are mounted via screws accessible from the underside of the baseplate.

The imaging CCD camera is mounted to the sidewall via a removable adapter ring. The ring allows for rotational and positional adjustment of the camera along the optical path. The adapter ring can be customized to accept other camera and mounting configurations. The spectroscopy CCD camera and re-imaging lens barrel are similarly mounted to a customizable adapter. This adapter, however, deliberately allows only rotational adjustment. A spacer ring is used to position the spectroscopy camera and subsequently the front of the lens assembly as close to the grating as possible while preventing contact of the lens barrel with the grating during lens focusing. Two cover plates located opposite each other on the spacer ring can be removed to gain access to the lens focus adjustment. A micrometer mounted to the spacer ring is interfaced to the spectroscopy camera adapter plate to allow for fine rotational adjustment of the camera. The spectroscopy CCD is located at a compound angle with respect to the baseplate. This angle was achieved by precision machining of the sidewalls; no angle adjustability was incorporated into the spectroscopy CCD mount assembly.

The instrument mounts to the telescope via a separate adapter plate. This allows easier installation and customization to different telescopes.

A sealed cabinet, separate from the main optical enclosure, houses the electronics. This cabinet bolts to the underside rails of the baseplate (see Figure 9), and connects via a cable harness to the spectrometer. When the electronics enclosure is removed, a set of four post mounts can be mounted to defined tie points on the rails to allow RITMOS to be operated on an optical table.

3.3. Electronic controls

As shown in Figure 10, the electronics cabinet houses the DMD controller boards, a microcontroller, the krypton calibration lamp and its power supply, and a filter wheel controller. The filter wheel system, an Oriel Electronics model 77371/77372, uses a proprietary digital interface that connects directly to the host PC.

A driving factor in the electronic design was the use of off-the-shelf components, while allowing remote operation from the telescope control room. The microcontroller is a good example. This multifunction board features signal conditioning, analog and digital I/O, and stepper control, and communicates with the host PC via a standard serial port interface. The microcontroller was chosen to allow flexibility for future modifications to the RITMOS electronics system. Not all functions of the board are utilized in the present design; currently it is used to toggle the calibration lamp assembly actuator and the lamp itself via solid-state relays, and to read a digital temperature monitor that is located inside the main optical cavity.

The DMD control electronics were supplied by Rochester MicroSystems, Inc. (RMI) in Rochester, NY. The DMD chip is rigidly clamp-mounted on a small carrier board, and connected via two ribbon cables to the electronics driver board, which is mounted in the electronics cabinet. The DMD electronics communicate with the host PC via a standard parallel port cable.

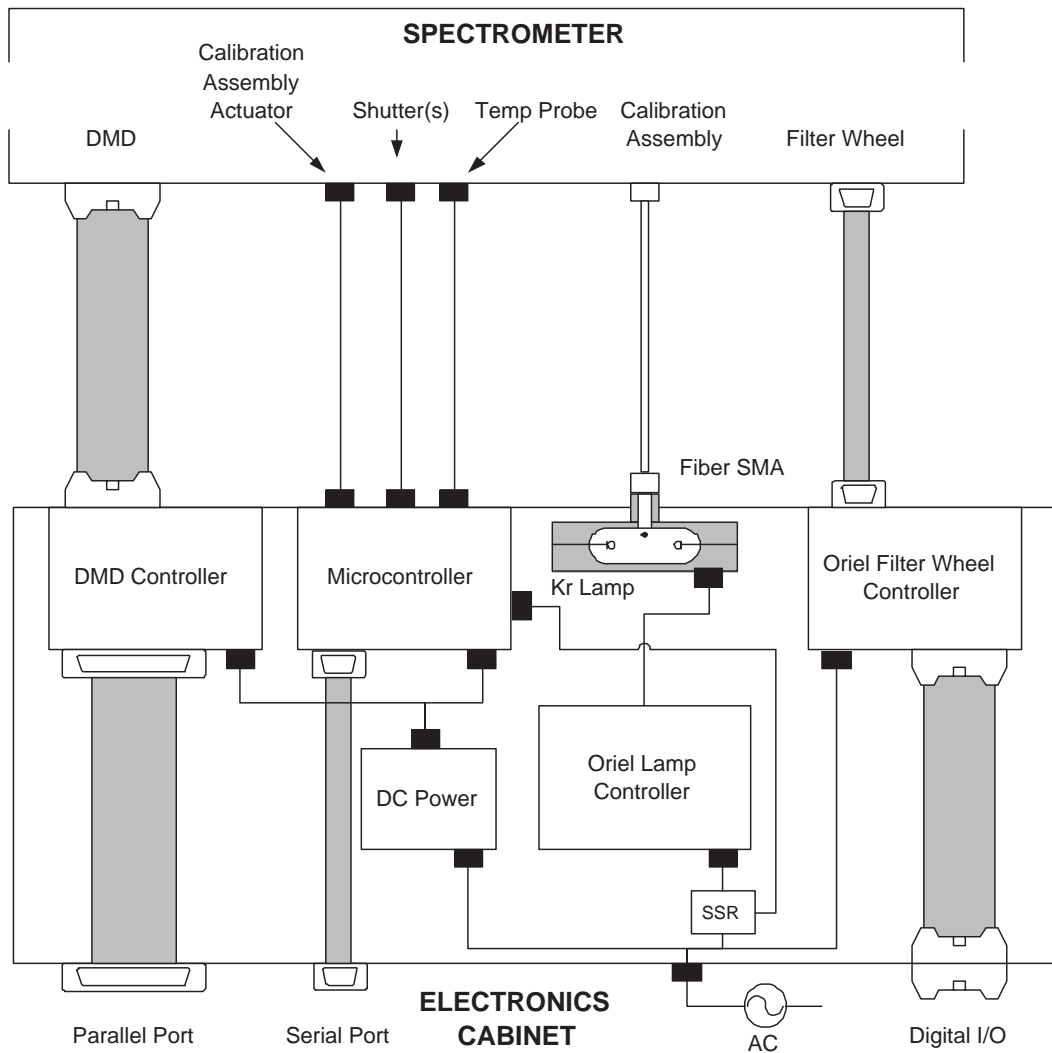


Figure 10. RITMOS electronics layout. Four nearly independent subsystems are aligned vertically in this schematic diagram; from left to right, they concern the DMD, the microcontroller, the calibration lamp, and the filter wheel. The microcontroller handles several miscellaneous duties for the user interface with which it communicates via an RS232 protocol. Its tasks include controlling the temperature probe, and toggling power to the krypton lamp and to the calibration assembly actuator through solid-state relays or SSRs. Also indicated are electrical connections for the optional future addition of shutters. The krypton lamp is coupled via a fiber-optic cable to the calibration assembly.

3.4. User Interface

The user controls the instrument through a standalone program, written specifically for RITMOS, that runs under Microsoft Windows. This program operates the DMD and the filter wheel, reads the onboard thermal sensor to display the current internal temperature, and switches the two elements of the calibration lamp assembly between their two available states. These two elements, the calibration lamp and its actuator, are independently addressable, although in normal operation the assembly will be “in position” when the lamp is on, and “out of position” when the lamp is off.

The control program allows both manual and automated reconfiguration of the DMD array. The user may “paint” on the DMD manually, and in real time if desired, by drawing on a canvas within the user interface; the control program then transfers this drawing to the DMD. Several basic painting tools are supported, and since

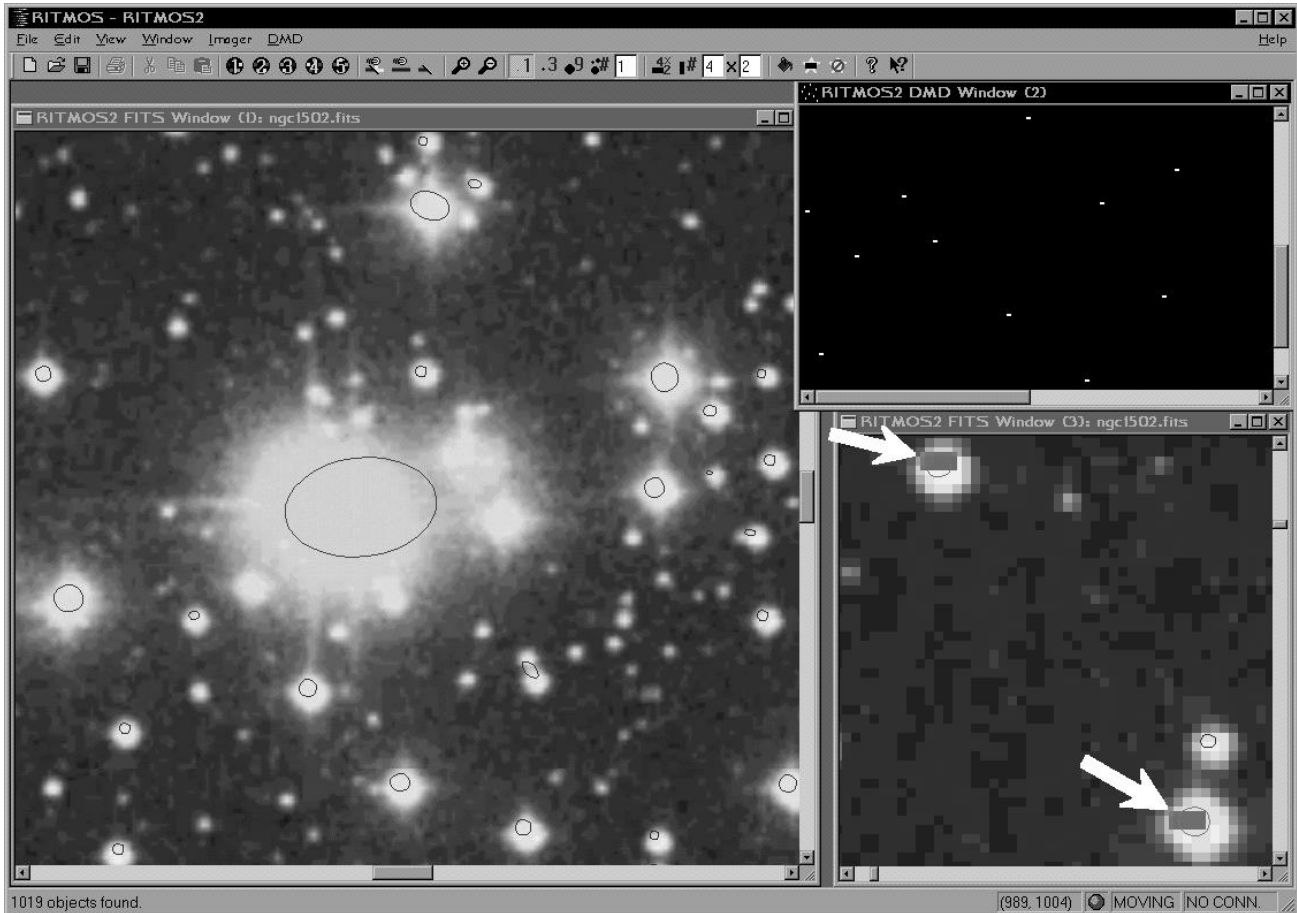


Figure 11. A screen snapshot of the user interface, version 0.12. The left window shows the center of a FITS image of NGC 1502, from the *Digitized Sky Survey* by way of an online database.¹⁵ The ellipses denote sources found by the detection and centroiding algorithm. The central stars were detected as one elongated ellipse due to blending in the image, but the algorithm assigned nearly circular ellipses to the more isolated stars. The upper right window shows a magnified region of the DMD canvas; the small white rectangles are 4×2 slits automatically placed over stars in the NGC 1502 image. The lower right window shows a highly magnified portion of this region, and includes the underlying FITS image. Overlaid white arrows mark slits that the program placed over two stars. Near the top of the main window, a row of buttons includes controls for the five-position filter wheel and the calibration lamp system, and tools for DMD slit construction and other forms of DMD painting.

the program imports and exports graphics in Windows monochrome BMP format, the user may opt to use an external drawing program. One of the basic painting tools is a filled rectangle or “slit.” A common application is to read in an exposure taken with the imaging camera, overlay a grid representing the DMD on top of this exposure, and to manually place slits at DMD pixels corresponding to interesting targets in the exposure. The user can thus manually, and by individual pixels if necessary, control exactly which areas of the field of view are deflected by the DMD to the spectroscopy channel.

The control program features an automated version of this process. Again an exposure from the imaging channel is imported, but now the software handles the process of identifying targets and placing rectangular slits at the appropriate DMD locations. The program detects and centroids sources in the image using algorithms derived from a centroiding routine developed by Terrence Girard of Yale University. The program computes the DMD location corresponding to each centroid, and places a slit there, avoiding spectral overlap by making sure the slit is separated from other slits in the transverse direction by a minimum number of DMD pixels. The selection routine also avoids sources that have already been observed, and there is an option to favor those sources

that are brighter and hence more likely to yield good spectra. The intent is to cover a field of, for example, open cluster stars in as few spectral exposures as necessary, and of course the user may modify the automated DMD configuration prior to observations.

The automated routines currently require further nights at the telescope to complete testing, but Figure 11 displays a snapshot of the user interface after execution of the routines as they stand now. The left window demonstrates source detection and centroiding, and the right windows demonstrate source selection, including spectral overlap avoidance. In the lower right window, notice the star directly above the bottom star in the window. The ellipse indicates the program detected this third star, but it chose not to place a slit there. Since the spectra are dispersed vertically relative to this window, a spectrum of the third star would contaminate that of the bottom star, so the third star must await a second spectroscopic exposure using a different slit pattern.

The nearly instantaneous refresh of the DMD, in combination with a quick imaging or spectral exposure, offers the user rapid feedback for the repositioning of slits. It takes about 0.5 seconds to completely update the 848×600 DMD array, which is obviously quite sufficient for astronomical spectroscopy. The Texas Instruments DMD itself is capable of much faster update rates, but the interface provided by RMI communicates via the control computer's parallel port, and is thus limited to about one megabit per second.

4. INITIAL MEASUREMENTS

The previous section discussed the performance expected from theoretical modeling of RITMOS. Now we consider experimental verification of these simulations, as well as general optical characterization of the instrument.

RITMOS requires two detectors for complete operation. For various reasons, a second CCD camera was either unavailable or inoperative for most of the time subsequent to the final assembly of RITMOS. Therefore, the tests undertaken thus far have usually only made use of the spectroscopy channel, to the neglect of, and without simultaneous information from, the imaging channel. A second CCD will be available shortly, and more comprehensive tests and observations will be presented in forthcoming papers. Nevertheless, some interesting results have been obtained, including the first multi-object spectroscopic observations acquired with a DMD-based MOS. These are presented in tandem with a study of the accuracy of their wavelengths. This section also concerns measurements of the plate scale and field of view at the DMD, flexure and temperature effects, spectral dispersion as a function of position on the focal plane, and delivered wavelength range.

The measurements were conducted at Mees Observatory. Figure 9 shows a photograph of RITMOS mounted to the 24" telescope.

4.1. Plate scale and field of view

As mentioned in §2, the theoretical plate scale of the Mees telescope at the Cassegrain focus is $25''/1/\text{mm}$; since the foreoptics in RITMOS converts the Mees telescope's $f/13.5$ beam to $f/7.62$, the plate scale on the DMD focal plane should be $44''/4/\text{mm}$, or $0''/755$ per $17 \mu\text{m}$ DMD pixel. From the multi-object spectroscopic observations of NGC 1502 that are discussed in §4.5, we inferred that the true plate scale is $0''/749 \pm 0''/008$ per DMD pixel. This estimate combined astrometry¹⁶ of the bright stars, their locations in the spectroscopic image, and the length of the DMD as faintly seen in the exposure; the latter quantity dominates the uncertainty. The theoretical and observed scales clearly agree within the measurement error. We expect a more precise estimate when the imaging channel becomes available with the second CCD camera.

The foreoptics barrel may be slid along the optical axis in order to adjust magnification modestly. In its current position, which is close to the nominal, the foreoptics illuminates the entire DMD except for a tiny piece of one corner. Thus, for all practical purposes, the field of view is 848×600 DMD pixels multiplied by the measured plate scale per pixel, or approximately $10/6 \times 7/5$. Vignetting due to the foreoptics is evident near the DMD edges.

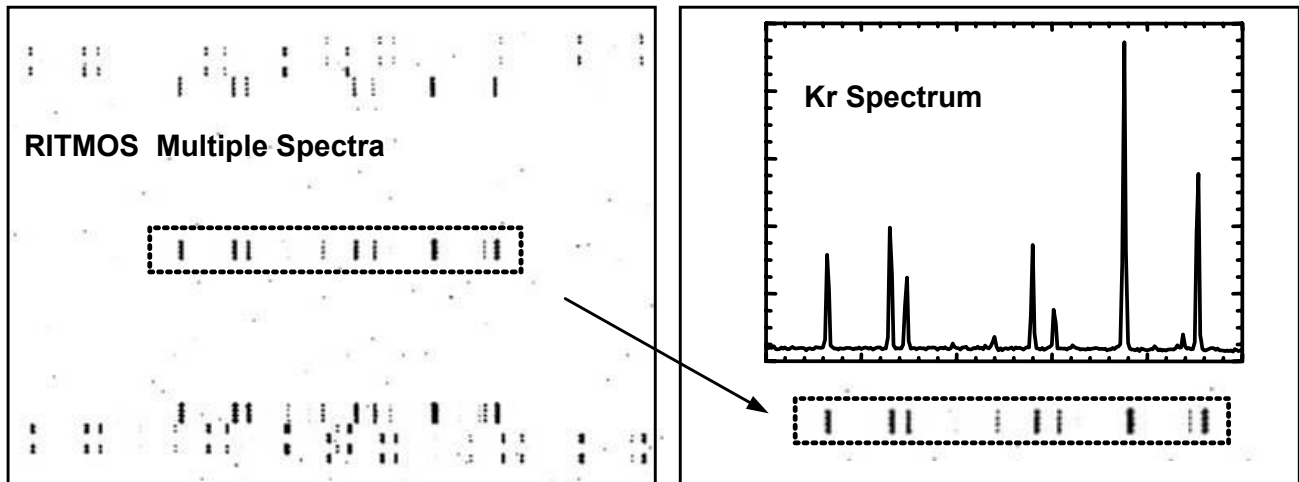


Figure 12. (Left) Raw spectroscopic image of krypton calibration lamp spectra taken with seven groups of slits arranged across the DMD. Each group consisted of four slits, each of which was 4×2 micromirrors in extent. The twenty-eight spectra are dispersed horizontally in this image, and are separated vertically; the slits were arranged to avoid overlap in the dispersion direction. The seven groups of spectra are shifted horizontally with respect to each other, because the slit groups occupy different areas of the DMD. (Right) A lineout from the central spectral group in the image. The bright blue emission lines of krypton, ranging from 4274.0 to 4502.4 Å, are evident.

4.2. Flexure and thermal effects

The effects of flexure and thermal variations are serious concerns for any spectrograph. Since RITMOS was not engineered in advance to exceed a specific tolerance on flexure or thermal distortions, it is especially necessary to ascertain their magnitudes through measurements. We constructed groups of slits at seven locations on the micromirror array: four groups near the corners, and three across the central region. With the krypton calibration lamp illuminating this pattern, we took spectroscopic exposures at various telescope pointings. One such exposure is Figure 12, which also shows a lineout from one of the groups of spectra. The exposures were taken from October through December of 2003 and thus also sampled a variety of temperatures; the temperature reported by the onboard sensor was recorded for each exposure.

We tracked the shift between exposures of seven of the brightest krypton wavelengths for each of the seven slit groups. For the flexure tests, the telescope was fixed at one declination (the observatory's latitude, $42^{\circ}42'$) and moved from -3^{h} to $+3^{\text{h}}$, thereby mimicking a 6^{h} track on a target. This may be a worst-case scenario, as a real observing program could schedule calibration exposures more often than once every six hours.

In the rotation from -3^{h} to $+3^{\text{h}}$, the seven groups of seven wavelength centroids shifted by an average of $4.4 \pm 0.3 \mu\text{m}$ in the dispersion direction on the spectroscopy focal plane. In the transverse direction, they shifted by an average of $1.87 \pm 0.08 \mu\text{m}$. The means and their errors are formal and represent the trend only; the shifts exhibited hysteresis and other nonlinear behavior. It is doubtful that the measurements can predict flexure-induced shifts, but the values are useful order-of-magnitude estimates. Significantly, a $4.4 \mu\text{m}$ shift is less than $1/3$ pixel for the $13.5 \mu\text{m}/\text{pixel}$ CCD for which the spectroscopy channel was designed. The engineering philosophy of using thick aluminum materials appears to have succeeded.

We similarly determined the average shift among the forty-nine wavelength centroids due to temperature variations. From the highest recorded temperature, $19^{\circ}03 \text{ C}$, to the lowest, $-5^{\circ}90 \text{ C}$, the spectra shifted by an average of $25.0 \pm 0.1 \mu\text{m}$ in the dispersion direction, and by an average of $7.3 \pm 0.3 \mu\text{m}$ in the transverse direction. Again, these are formal values only, and nonlinear behavior underlies these shifts as well. Since a real spectroscopic observation will likely not experience a temperature change of $\sim 25^{\circ} \text{ C}$, the actual magnitude of spectral shifts should be far less in practice.

4.3. Spectral dispersion

The calibration lamp exposures described in §4.2, of which Figure 12 is an example, can also be used to calculate the spectral dispersion as a function of position on the spectroscopy focal plane, or equivalently as a function of micromirror position. One of the slit groups is at the center of the DMD, and four others are very close to the corners (five pixels from the DMD edge, in the dispersion direction). For each of these five slit groups, we fitted a polynomial to the seven brightest krypton line centroids. We conducted these fits for eleven of the exposures described in §4.2, and averaged the results. We also fitted polynomials to dispersion predictions generated by the ZEMAX optical model. In all cases, we found the polynomial terms above the linear term to be extremely small. Table 2 lists the best-fit coefficients, and their errors, for quadratic fits to the five slit groups. For each group, the table also lists the dispersion, which is the inverse of the linear coefficient. The difference between prediction and reality for each slit group is well within expectations.

Table 2. Spectral dispersion, from fits to positions on the spectroscopy focal plane, for light from the DMD center (position #3) and the four corners. Positions #1 and #2 share the same long edge, and #4 and #5 share the other long edge, of the DMD. The dispersion is parallel to the short edges. The fit has the functional form $y = a_0 + a_1x + a_2x^2$, where $x \equiv \lambda - 4400 \text{ \AA}$. “Theoretical” lines refer to ZEMAX predictions, and “observed” lines to the equivalent points in the calibration lamp exposures discussed in §4.2.

DMD position	a_0 (mm)	a_1 (mm/Å)	a_2 (mm/Å ²)	dispersion ($1/ a_1 $) (Å/mm)
1 (theoretical)	-2.257 ± 0.006	-0.020691 ± 0.000012	$(-5.2 \pm 0.4) \times 10^{-7*}$	48.33 ± 0.03
1 (observed)	-1.8643 ± 0.0004	-0.020527 ± 0.000003	$(-3.7 \pm 0.5) \times 10^{-7}$	48.717 ± 0.008
2 (theoretical)	-2.251 ± 0.006	-0.020692 ± 0.000012	$(-5.2 \pm 0.4) \times 10^{-7*}$	48.33 ± 0.03
2 (observed)	-1.8324 ± 0.0003	-0.020519 ± 0.000002	$(-3.0 \pm 0.3) \times 10^{-7}$	48.735 ± 0.005
3 (theoretical)	-0.004 ± 0.006	-0.020588 ± 0.000012	$(-3.7 \pm 0.4) \times 10^{-7*}$	48.57 ± 0.03
3 (observed)	0.3492 ± 0.0004	-0.020428 ± 0.000003	$(-2.1 \pm 0.5) \times 10^{-7}$	48.953 ± 0.008
4 (theoretical)	2.204 ± 0.006	-0.020535 ± 0.000013	$(-2.2 \pm 0.5) \times 10^{-7*}$	48.70 ± 0.03
4 (observed)	2.4970 ± 0.0004	-0.020393 ± 0.000003	$(-1.8 \pm 0.5) \times 10^{-7}$	49.037 ± 0.008
5 (theoretical)	2.204 ± 0.006	-0.020536 ± 0.000013	$(-2.2 \pm 0.5) \times 10^{-7*}$	48.69 ± 0.03
5 (observed)	2.5289 ± 0.0003	-0.020389 ± 0.000003	$(-0.7 \pm 0.4) \times 10^{-7}$	49.046 ± 0.006

*According to the fitting routine, the IDL¹⁷ routine “SVDFIT,” this term was consistent with zero.

4.4. Delivered wavelengths

Table 1 specifies 4400 \AA as the central wavelength of the minimum delivered wavelength range, which is $3900\text{--}4900 \text{ \AA}$. The fit to the observation of position #3 (see Table 2) indicates that 4400 \AA is approximately 350 microns from the center of the spectroscopy CCD, or ~ 26 pixels for a $13.5 \mu\text{m}$ format detector.

The CCD that was available for the observations at Mees has a 512×512 format with $24 \mu\text{m}$ pixels. It is not large enough to confirm the full delivered wavelength range; however, Table 2 indicates that it should capture the central $4100\text{--}4700 \text{ \AA}$, for pixels near the center of the micromirror array. The stellar spectra presented in the next section show that the approximate range $4100\text{--}4700 \text{ \AA}$ is delivered to the CCD. For example, $\text{H}\delta$, at 4102 \AA , is visible in one of the spectra.

4.5. Multi-object spectra

Figures 13 and 14 show multi-object spectra of the center of the open cluster NGC 1502, taken with RITMOS. As mentioned in §4.4, the CCD used for these observations has a 512×512 format with $24 \mu\text{m}$ pixels, and therefore only captures the approximate wavelength range $4100\text{--}4700 \text{ \AA}$. Nevertheless, several absorption features are obvious in the 5 minute exposure plotted in Figure 14a. Figure 14c demonstrates the ability to place slits on the DMD and thereby select certain targets, in this case three stars, for simultaneous spectral acquisition.

The signal-to-noise ratio in Figure 14c is lower than in Figure 14a because the narrow slits used in Figure 14c intercepted only a small part of the stars’ broad seeing disks; telescope tracking errors, unrelated to RITMOS,

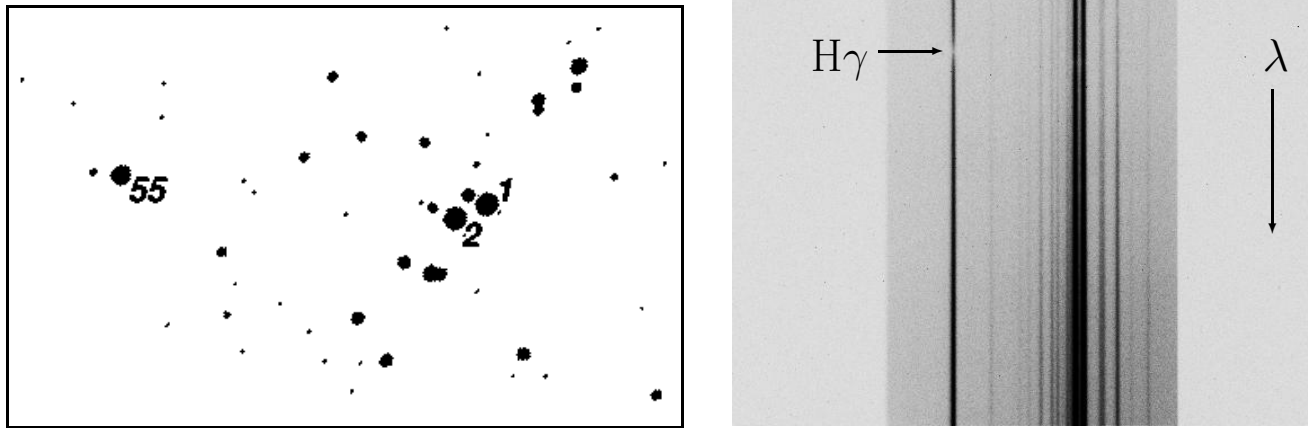


Figure 13. The central region of the open cluster NGC 1502. The chart on the left was generated by WEBDA,¹⁸ and then rotated and scaled to map horizontally to the spectral image on the right. The spectra in the image are dispersed vertically and cover approximately 4100–4700 Å. The image, unprocessed except for cosmic ray removal, is a spectroscopic CCD exposure of the field in the star chart, and was taken with the entire micromirror array in RITMOS tilted towards the spectroscopy channel. More than a dozen stellar spectra are present; the three deepest correspond to the three brightest stars in the star chart, which are labelled with their NGC 1502 catalog numbers as assigned by WEBDA and by Purgathofer.¹⁹ Star #55, corresponding to the leftmost of the three deep spectra, is HD 25594, an A0(V) star (perhaps²⁰ A2Vn) with $B = 7.99$, according to SIMBAD¹⁶; the absorption feature clearly present in its spectrum is H γ . Star #1 is HD 25638 with $B = 7.41$, and #2 is HD 25639 with $B = 7.26$; both have approximately B0III spectral types.^{16, 18} The spectral image is a 5 minute exposure taken with the Mees 24" telescope under light clouds on 2004 Jan. 10.

caused the stars to drift rapidly out of these slits; and the combination of three CCD exposures increased the total readout and background noise. Clearly the use of the instrument on a telescope with better tracking and at a site with better seeing would substantially improve the detected signal.

4.6. Wavelength calibration

Figure 14c, in conjunction with the catalog spectra of Figure 14b, also demonstrates the ability of the onboard krypton lamp assembly to calibrate the wavelengths of spectral features.* The spectra in Figure 14c were transformed to wavelength space by taking a second spectroscopic exposure with the same slit pattern illuminated by the krypton lamp instead of the sky. The mapping from pixels to wavelengths was computed from the observed krypton lines, and applied to the stellar spectra, yielding absorption features that line up with their counterparts in the catalog spectra to within 1 Å. Apart from possible binary star variations, the spectra have been corrected for topocentric radial velocities, even though the velocity shifts are small, being less than 0.5 Å at 4400 Å.

5. CONCLUSION

We have constructed a multi-object spectrograph that utilizes a novel technique for target selection—a micromirror array replaces the conventional slit mask or fiber bundle at the telescope focal plane. This first-generation DMD-based MOS has been designed for moderate dispersion at blue wavelengths, making it favorable for multi-object MK spectral classification. We have detailed the optical, mechanical, electronic, and software designs, and

*Figure 14a, unlike Figure 14c, was shifted in wavelength manually, because no lamp exposures were taken in conjunction with the spectra of Figure 14a, and telescope drift rendered the lamp exposures for Figure 14c inapplicable to Figure 14a.

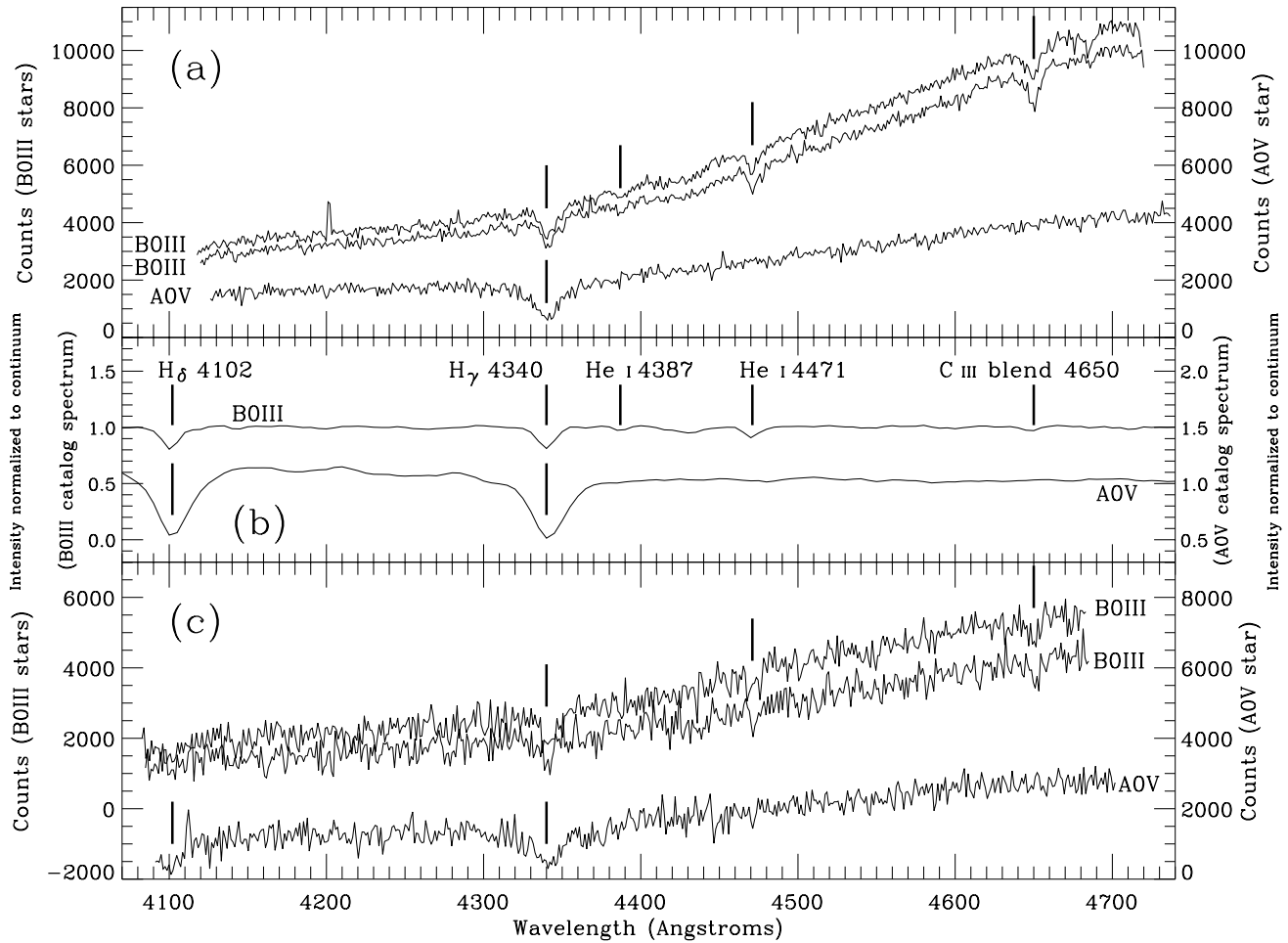


Figure 14. Spectra of three stars in the central region of NGC 1502, as measured with RITMOS. **(a)** The three brightest spectra from Figure 13, with counts for the two B0III stars and the A0V star indicated along the left-hand and right-hand axes, respectively. The background (sky) and most cosmic ray hits have been subtracted, but the spectra have not been flux-calibrated. Visible in this 5 min. exposure are all of the obvious features in the catalog spectra of part (b); these features are noted with vertical lines. **(b)** Catalog spectra, from the spectral library of Ref. 21, with intensity normalized to the continuum, such that 0 indicates no signal and 1 is the continuum level. The left-hand and right-hand axes denote the interpolated B0III and A0V catalog entries, respectively. The five most obvious spectral features are marked with vertical lines. **(c)** Similar to part (a), except that three-pixel-wide slits were placed on the DMD across each star's location, and that it is a combination of three exposures, for a total of 21 min., under the same observing conditions. The visible spectral features from part (b) are noted with vertical lines.

have presented simulation predictions of the optical performance. We have compared some of these predictions to measurements at the telescope and have found excellent agreement. We have also demonstrated the primary function of the instrument by acquiring multiple stellar spectra simultaneously.

A future paper will focus on optical characterization, including measurements of throughput and MTF, and a study of the scattering which is induced by the DMD properties mentioned in §1. Another paper will concentrate on astronomical performance, and will present open cluster multi-object spectra taken with a new Spectral Instruments camera that features a Fairchild 486 CCD with 4096×4096 $15 \mu\text{m}$ square pixels, $\sim 3.3 e^-$ read noise, and $\sim 80\%$ quantum efficiency around 4400 \AA .

ACKNOWLEDGMENTS

We thank Terry Girard of Yale University for the star detection and centroiding algorithms in the user interface, R. Scott Russell of Eastman Kodak for gracious assistance with observations, and Robert Slawson of R.I.T. for helpful discussions. Albert Piterman of Pixel Physics provided data reduction for the investigation of flexure and thermal effects. We thank our colleagues in the University of Rochester Departments of Physics and Astronomy, and in particular Prof. William Forrest, for allowing us continuing access to Mees Observatory. Z.N. would like to thank Prof. Gordon Walker of the University of British Columbia who introduced him to the issues of multi-object spectroscopy during a summer stay in the Department of Geophysics and Astronomy. This research was supported by a New York State Center for Advanced Technology grant to the Center for Electronic Imaging Systems, and a National Science Foundation Small Business Innovative Research (SBIR) grant to Pixel Physics.

REFERENCES

1. L. J. Hornbeck, "Digital Light Processing: A New MEMS-Based Display Technology," in *Technical Digest of the IEEE 14th Sensor Symposium*, pp. 297–304, Kawasaki, Japan, 1996.
2. M. R. Douglass, "Lifetime Estimates and Unique Failure Mechanisms of the Digital Micromirror Device (DMD)," in *1998 IEEE International Reliability Physics Symposium Proceedings*, pp. 9–16, 1998.
3. A. Dey, "The Future of Wide-Field Multi-Object Spectroscopy," in *Next Generation Wide-Field Multi-Object Spectroscopy*, M. J. I. Brown and A. Dey, eds., *A. S. P. Conf. Ser.*, **280**, pp. 7–12, 2002.
4. J. W. MacKenty, M. A. Greenhouse, R. F. Green, L. M. Sparr, R. G. Ohl, and R. S. Winsor, "IRMOS: An Infrared Multi-Object Spectrometer using a MEMS micromirror array," in *Instrument Design and Performance for Optical/Infrared Ground-based Telescopes*, M. Iye and A. F. M. Moorwood, eds., *Proc. SPIE*, **4841**, pp. 953–961, 2003.
5. K. J. Kearney and Z. Ninkov, "Characterization of a digital micromirror device for use as an optical mask in imaging and spectroscopy," in *Spatial Light Modulators*, R. L. Sutherland, ed., *Proc. SPIE*, **3292**, pp. 81–92, 1998.
6. R. L. Davies *et al.*, "GMOS: the GEMINI Multiple Object Spectrographs," in *Optical Telescopes of Today and Tomorrow*, A. L. Ardeberg, ed., *Proc. SPIE*, **2871**, pp. 1099–1106, 1997.
7. I. M. Hook, J. R. Allington-Smith, S. Beard, D. Crampton, R. Davies, C. J. Dickson, A. Ebbers, M. Fletcher, I. Jørgensen, I. Jean, S. Juneau, R. Murowinski, R. Nolan, K. Laidlaw, B. Leckie, G. E. Marshall, T. Purkins, I. Richardson, S. Roberts, D. Simons, M. Smith, J. Stilburn, K. Szeto, C. J. Tierney, R. Wolff, and R. Wooff, "Gemini-north multiobject spectrograph integration, test, and commissioning," in *Instrument Design and Performance for Optical/Infrared Ground-based Telescopes*, M. Iye and A. F. M. Moorwood, eds., *Proc. SPIE*, **4841**, pp. 1645–1656, 2003.
8. *GMOS: Multi-Object Spectroscopy*, <http://www.gemini.edu/sciops/instruments/gmos/gmosMOS.html>, 2004.
9. S. C. Barden and T. Armandroff, "Performance of the WIYN fiber-fed MOS system: Hydra," in *Fiber Optics in Astronomical Applications*, S. C. Barden, ed., *Proc. SPIE*, **2476**, pp. 56–67, 1995.
10. D. Harmer, private communication to R. Meyer, 2004.
11. A. B. Sontheimer, "Digital Micromirror Device (DMD) Hinge Memory Lifetime Reliability Modeling," in *2002 IEEE International Reliability Physics Symposium Proceedings*, pp. 118–121, 2002.
12. *WIYN Observatory: WIYN Facts*, <http://www.noao.edu/wiyn/wiynfacts.html>, 2004.
13. A. Offner, "Unit Power Imaging Catoptric Anastigmat," U.S. Patent 3,748,015, 1973.
14. J. Allington-Smith, "Basic equations for astronomical spectroscopy with a diffraction grating," available at <http://aig-www.dur.ac.uk/fix/projects/dispersion/dispersion.html>, 2000.
15. L. Boyle and K. Janes, *Boston University Open Cluster Database*, <http://astro.bu.edu/ocl>, 2004.
16. *SIMBAD Astronomical Database*, <http://simbad.u-strasbg.fr/Simbad>, 2004.
17. *IDL: The Interactive Data Language*, <http://www.rsinc.com/idl>, 2004.
18. J.-C. Mermilliod, *WEBDA: A Site Devoted to Stellar Clusters*, <http://obswww.unige.ch/webda>, 2004.
19. A. Purgathofer, "Dreifarbenphotometrie in offenen Sternhaufen sowie in zwei Sternfeldern im Cyg.," *Ann. Univ. Sternw. Wien*, **26**, pp. 37–73, 1964.
20. A. A. Hoag and N. L. Applequist, "Distance Moduli of Open Clusters," *Ap. J. Suppl.*, **12**, 215–237, 1965.
21. A. J. Pickles, "A Stellar Spectral Flux Library: 1150–25000 Å," *Publ. A. S. P.*, **110**, pp. 863–878, 1998.